Journal of Alloys and Compounds 509 (2011) 6481–6488

Contents lists available at ScienceDirect

Journal of Alloys and Compounds

journal homepage: www.elsevier.com/locate/jallcom

Twinning, grain orientation and texture variation of AZ31 Mg alloy during compression by EBSD tracing

Guang-Sheng Song[a,b], Shi-Hong Zhang[a,*], Li Zheng[a], Liqun Ruan[c]

[a] Institute of Metal Research, Chinese Academy of Sciences, Shenyang, China
[b] School of Materials Science and Engineering, Shenyang Aerospace University, Shenyang, China
[c] Department of Industrial Science, Kumamoto University, Kumamoto, Japan

ARTICLE INFO

Article history:
Received 18 November 2010
Received in revised form 17 March 2011
Accepted 17 March 2011
Available online 29 March 2011

Keywords:
Mg alloy
Grain orientation
Extension twin
Basal slip
Twin variant
Schmid factor

ABSTRACT

In order to investigate the micro-mechanism of warm forming of Mg alloys, three specimens cut from a rolled AZ31 sheet were chosen to be compressed along the Rolling Direction (RD) at 100 °C, 170 °C and 230 °C, separately. During compression, an in situ measurement of grain orientation in the plane of RD × TD (Transverse Direction) was carried out with EBSD method. Experimental and analytical results show that temperature has remarkable impact on activation of twinning and variation of texture. As the temperature was raised from 100 °C to 230 °C, the number of grains with twins activated decreased substantially during deformation, and rolling texture varied from quick vanishing at 100 °C to always existing at 230 °C. Tracing for orientation of individual grains during deformation shows that there are obvious different orientation changes between grains with twins activated and those without twins activated. Twinning plays a significant effect on texture variation during compression. The extension twin variant really activated during deformation is the one with maximal Schmid factor.

1. Introduction

Mg alloys are promising metallic materials for structural applications due to their low density and high specific strength, while research activities regarding plastic forming technique of Mg alloys have been surging in recent years. However, die casting is still the main technique for producing Mg alloys parts up to now, in which process defects are hard to be avoided, such as shrinkage porosity, shrinkage void and relatively low strength. Plastic forming technology is an alternative for Mg alloy casting to avoid above defects. While as a hexagonal close-packed (hcp) metal, Mg alloys have poor formability at room temperature due to insufficient number of independent slipping systems.

Since the formability of Mg alloys is poor at room temperature, raising deformation temperature may be the easiest way to improve their formability. The melting temperature of magnesium is about 650 °C, thus the deformation temperature of magnesium alloys will be remarkably lower than this value, and deformation at temperature over 350 °C should usually be classified as high temperature deformation for Mg alloys. Taking into account the poor oxidation resistance of Mg alloys and the high costs for production, high temperature was not suitable for sheet metal processes, other than for hot rolling and hot extrusion when high temperature is a necessity. Warm forming of Mg alloys is attracting more and more attentions from researchers [1–4] as a newly developed plastic forming technology in recent years, due to its advantages of avoiding poor formability at room temperature and over-oxidization at high temperature simultaneously. Specifically, warm forming of Mg alloys usually means that the deformation temperature is below 250 °C [5,6].

As a newly developed technology of texture measurement in recent twenty years, the Electron Backscatter Diffraction (EBSD) technique could measure metal texture on the individual grain scale, and possesses higher precision than XRD for texture measurement on the micro-scale, the EBSD method has thus been used for studying the deformation technique of the Mg alloys by many researchers in recent years [7–28]. Up to now, research activities on the formability of Mg alloys are mainly focused on the processes of the Equal-Channel Angular Pressing (ECAP)[14,20,29], uniaxial tension [9,12,13,22] or compression [12,15,16,22,30], rolling [10,11,19,23,25,26], special extrusion [17,28,31], twin roll casting (TRC) [32,33], etc., and related deformation mechanisms studied in their work are mainly about Dynamic Recrystallization (DRX) [10,20,24,27–32], superplasticity [14,27,33] and activations of slip system and twinning [16–18,25]. Among the numerous papers cited above, though some researches are related to investigations on the micro-mechanism of warm forming of magnesium alloys, there are no reports on tracing variations of texture on individual grains scale, this is maybe because deformation temperature is higher than the temperature of recrystallization in many

* Corresponding author. Tel.: +86 24 83978266.
E-mail address: shzhang@imr.ac.cn (S.-H. Zhang).

0925-8388/$ – see front matter © 2011 Elsevier B.V. All rights reserved.
doi:10.1016/j.jallcom.2011.03.106

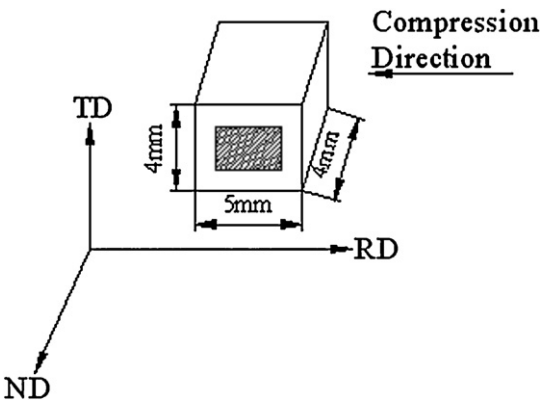

Fig. 1. Schematic illustration of the specimen for compression and EBSD.

experiments and this makes it hard to trace individual grains, or there are many inconveniences for realizing this process in the experiments.

In the experiments and research reported in the present article, an in situ measurement of grain orientation of AZ31 magnesium alloy in the plane of RD × TD during deformation was carried out by using the EBSD method under conditions of compression at 100 °C, 170 °C and 230 °C, separately. The aim is to reveal the micromechanism of warm deformation on individual grain scale.

2. Experimental details

Fig. 1 shows the AZ31 magnesium alloy specimen cut from a rolled AZ31 sheet (the rolling process: a 6 mm thick extruded blank was rolled into a 4 mm thick sheet with 0.6 mm pass reduction at 400 °C), the dashed region in the plane of RD × TD is the region where the texture is measured with EBSD method. Specimens prepared for EBSD measurement were ground by carbide silicon sand paper and mechanically polished by velour, and then electro-polished in a solution of 10% perchloric acid and ethanol solution, chilled to −30 °C, using a 15 V potential. The texture measurements were carried out by using a JECOL6500F field emission SEM equipped with a HKL Channel 5.0 software, the scanning step size is 1.5 μm and the magnification is 300.

Under the conditions of 1.0×10^{-3} Pa vacuum and 0.1 mm/min compression velocity, three specimens were compressed uniaxially on a Gleeble1500 thermal simulator at temperatures of 100 °C, 170 °C and 230 °C, separately. For every specimen, the texture in the selected region was measured with EBSD method before compression, then the specimen was compressed to a strain along the direction as shown in Fig. 1. After this deformation, the specimen was unloaded from the Gleeble1500 and the texture in the same region was measured with EBSD method again. In this way, this specimen was subsequently compressed and measured for other two times in the following steps, i.e. every specimen was compressed to three different strains, four EBSD measurements were carried out correspondingly (including measurement before compression). In the experiments, three Vickers hardness marks were separately made on the three corners of the rectangular scanning region in the plane of RD × TD for every specimen, which aims to keep every EBSD measurement to be carried out in the same region, as shown in Fig. 1.

3. Results and discussion

3.1. Deformation textures

For the specimen compressed at 100 °C, the grain orientations in the same measured region at different strains are shown in Fig. 2, 20 complete grains numbered from 1 to 20 could be traced in the measured region throughout the deformation process. Colors representing grain orientations in Fig. 2 are obviously different between the orientation without height reduction and that with height reduction of 7.5%. On the contrary, there are almost no differences for colors in orientation maps related to height reductions of 7.5%, 11% and 13.6%, which means that there are many changes of grains orientation for compression from 0% to 7.5% but less from 7.5% to 13.6%.

Changes of texture during deformation could be illustrated explicitly by pole figures in Fig. 3, where typical basal texture exists

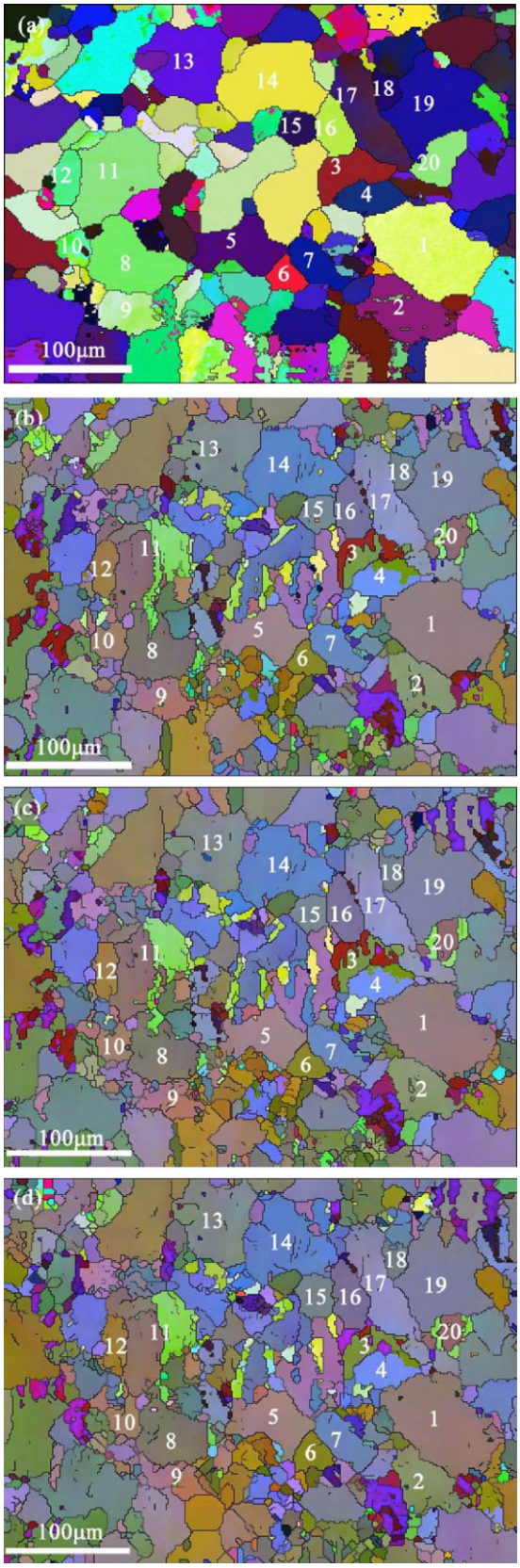

Fig. 2. Orientation micrograph of grains at different strains during compression at 100 °C, (a) 0%, (b) 7.5%, (c) 11% and (d) 13.6%.

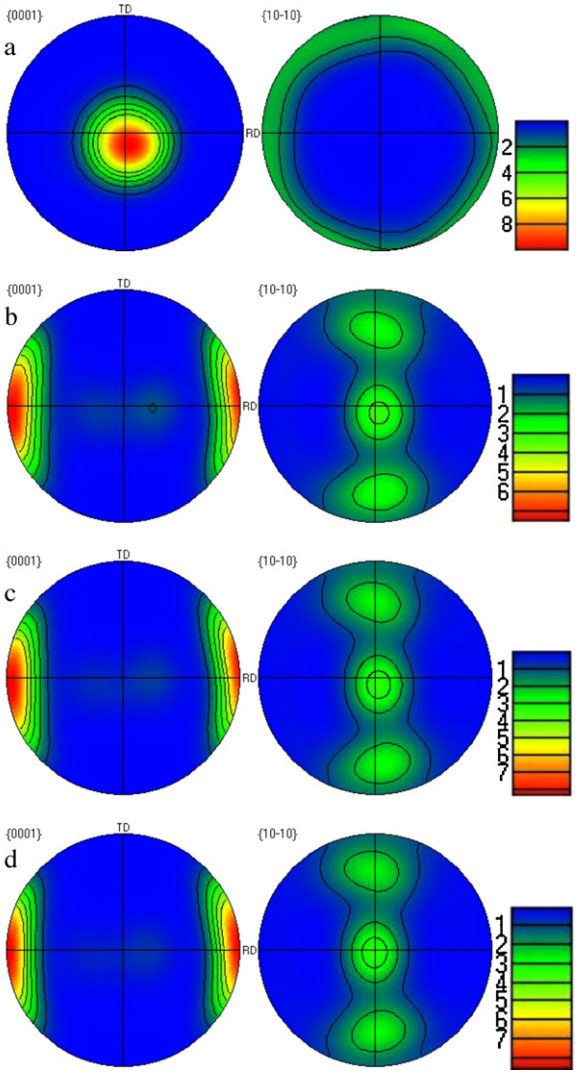

Fig. 3. Pole figures of the specimen compressed to different strains at 100 °C, (a) 0%, (b) 7.5%, (c) 11% and (d) 13.6%.

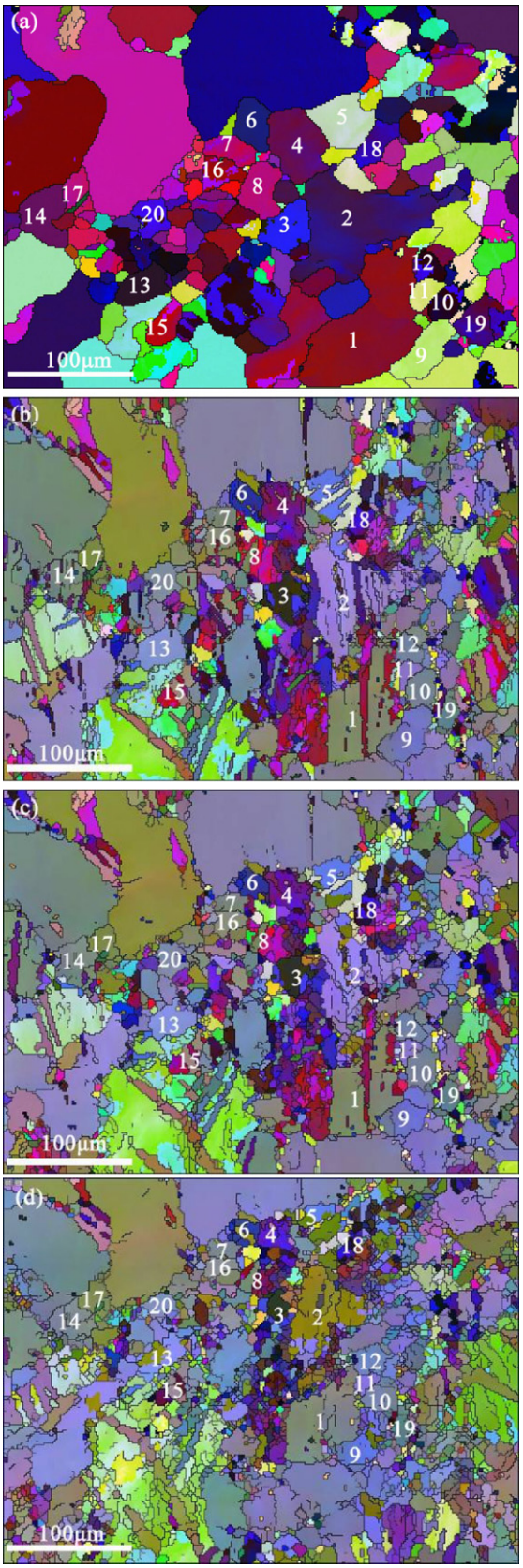

Fig. 4. Orientation micrograph of grains at different strains during compression at 170 °C, (a) 0%, (b) 11%, (c) 16.4% and (d) 24.5%.

for the rolled specimen (0% height reduction), which means most grains with their *c*-axes parallel to the ND (Normal Direction), but the basal texture has vanished after 7.5% compression, and the *c*-axes of most grains are inclined to the RD (the direction of compression), while there are almost no changes of pole figures after 11% and 13.6% compression.

Among the deformation modes of Mg alloys, twinning can change grain orientations considerably, but basal, prismatic and pyramidal slips can hardly change grain orientations during deformation, so it can be concluded that twinning may be activated when the specimen was compressed from 0% to 7.5%. In view of the relationship of twinning modes, the initial texture and the compression direction, extension twins can activate during this deformation process. Pyramidal slips cannot activate during this deformation because the deformation temperature is lower than 225 °C [28], and prismatic slips usually cannot activate when deformation at 100 °C, so we can also conclude that, for compression from 7.5% to 13.6%, basal slips should be the main deformation mode.

Among the 20 grains numbered in Fig. 2, and according to the variations of grain orientation from 0% to 7.5%, for grains 3, 11 and 20, only part of the whole grain matrix might have transformed into twinning from 0% to 7.5% strain, but for other 17 grains, maybe the whole grain matrix have transformed into twinning.

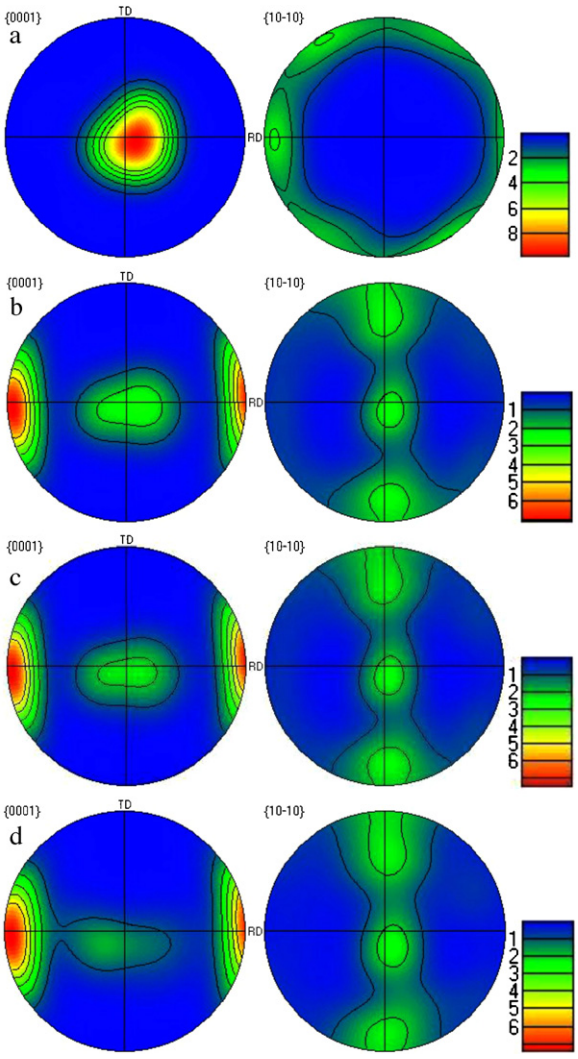

Fig. 5. Pole figures of the specimen compressed to different strains at 170 °C, (a) 0%, (b) 11%, (c) 16.4% and (d) 24.5%.

Variations of grain orientation during compression at 170 °C are shown as Fig. 4. Similarly as compression at 100 °C, there are obvious differences for grain orientations during compression from 0% to 11%, but almost no variations for strain from 11% to 26.4%. Just as compression at 100 °C, 20 complete grains could be traced in the measured region throughout the deformation process, which are also numbered from 1 to 20. Among them, for grains numbered 1, 2, 3, 5, 6, 8, 15 and 19, only part of the their grain matrix might have transformed into twinning from 0% to 11% strain, but for other 13 grains, maybe the whole grain matrix have transformed into twinning.

Variations of texture during compression at 170 °C are shown as Fig. 5, that was different from compression at 100 °C. The basal texture had not vanished fully after 11% compression, but vanished steadily after 24.5% compression. This can be explained by comparing the characteristics of twinning activation for compression at 100 °C and 170 °C. As introduced above, for the chosen twenty grains in the scanning region compressed at 100 °C, most grain matrix had entirely transformed into twinning after the specimen was compressed to 7.5% strain, but for compression at 170 °C, most grain matrix transformed partly into twinning after the specimen was compressed to 11% strain.

Fig. 6 shows variations of grain orientation during compression at 230 °C, that was clearly different from compression at 100 °C

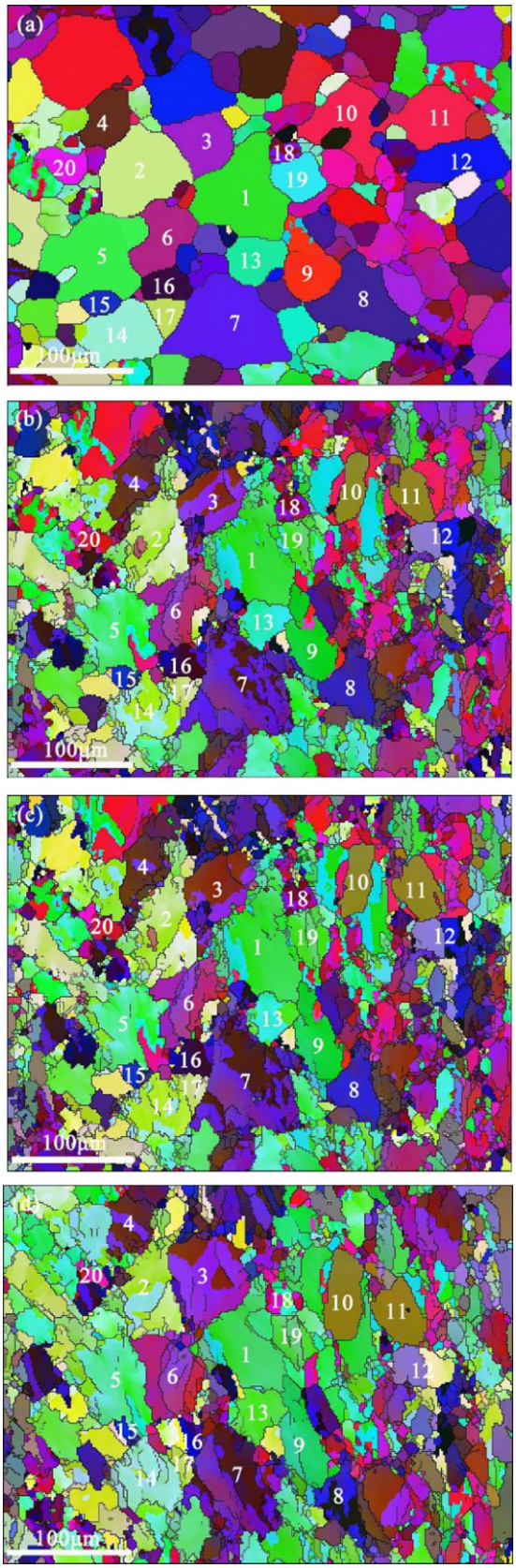

Fig. 6. Orientation micrograph of grains at different strains during compression at 230 °C, (a) 0%, (b) 11.3%, (c) 19% and (d) 26.9%.

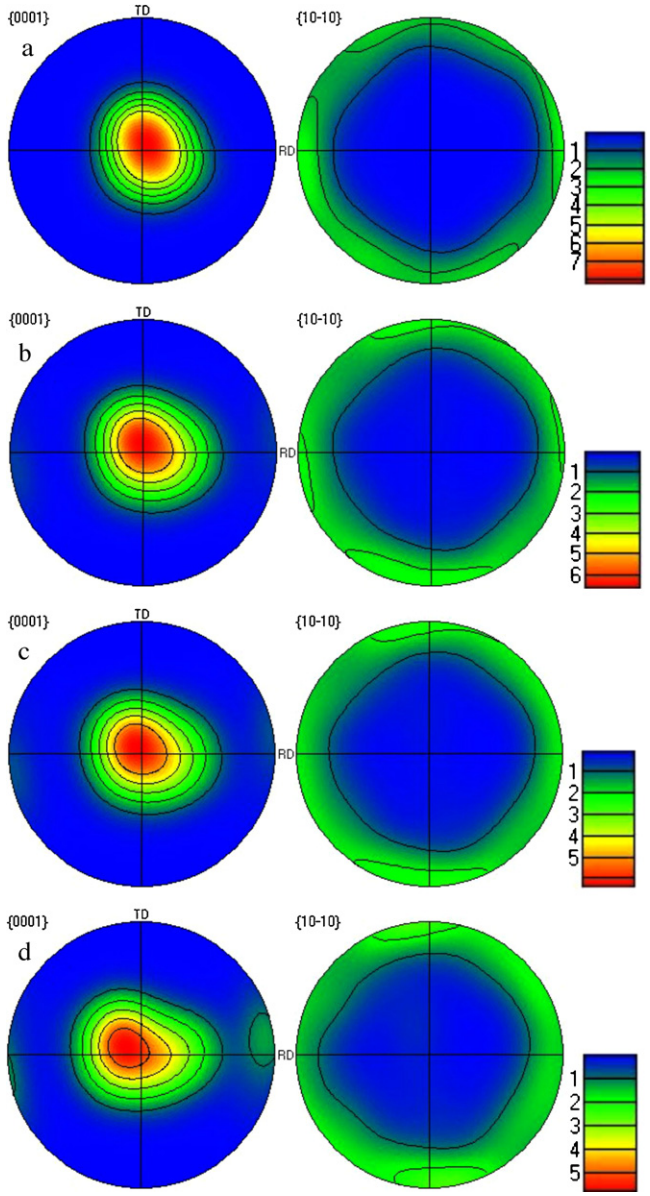

Fig. 7. Pole figures of the specimen compressed to different strains at 230 °C, (a) 0%, (b) 11.3%, (c) 19% and (d) 26.9%.

Table 1
Extension twin variants of grains 1–9 at 100 °C.

Grain No.	1	2	3	4	5	6	7	8	9
Twin variant	TT2	TT4	TT4	TT6	TT6	TT1	Null	TT3	TT3

and 170 °C, there are almost no changes of grain orientations after compression from 0% to 26.9%. Fig. 7 shows the variations of texture during the deformation process, basal texture was not weakened clearly during the whole deformation. Accordingly, we can conclude that there should be almost no twins activated during the whole deformation for most grains.

In Fig. 6, there are only grains 9, 10 and 11, in which part of the grain matrix might have transformed into twinning among the 20 grains chosen to trace variations of grain orientations, and twinning did not activate during the deformation process for the other 17 grains.

3.2. Extension twin variants

As a kind of hexagonal close packed (hcp) metal, twinning is an alternative deformation mode for Mg alloys, especially at the initial phase of compression deformation. For the rolled Mg alloy sheets, extension twins will activate if they are compressed along RD due to the existence of typical basal texture. Taking into account the symmetry of hcp, there will be six twin variants for extension twins in which three are independent. For an individual grain, if the orientation corresponding to the initial state (before deformation) is measured, based on the misorientation relationship of $86.3^\circ/\langle 1\,1\,\bar{2}\,0\rangle$ (86.3° is rotation angle and $\langle 1\,1\,\bar{2}\,0\rangle$ is rotation axis), the orientations of the six extension twin variants will be determined after deformation, and each of them is compared with the measured orientations of the same grain corresponding to a strain, then six misorientation values will be obtained, in which, the twin variant corresponding to the minimal misorientation value is the one that really activates during deformation.

For the specimen compressed at 100 °C, based on the measured orientations corresponding to the strain of 0% and 7.5%, the first 9 grains (numbered from 1 to 9 in Fig. 2) in the scanning region were chosen to determine their extension twin variants by means of the procedure introduced above. The corresponding calculation results are listed in Table 1, in which the extension twin variants are presented by combining two letters of "TT" with one number, in which "TT" means extension twin and the number means the corresponding number in the six extension twin variants shown in Table 2. There are no extension twins activated during deformation (twin variant null) for grain 7.

The {0 0 0 1} pole figures for each of the above 9 grains are shown in Fig. 8 (Fig. 8(1)–(9) was correspondingly {0 0 0 1} pole figures of grains 1–9 in Fig. 2). In every figure, the points marked with 0%, 7.5%, 11% and 13.6% represent the corresponding strains, while the points marked with symbols of t1–t6 represent distributions of extension twin variants of the corresponding grain matrix (before deformation). As shown in Fig. 8, in {0 0 0 1} pole figures of every grain (the {0 0 0 1} pole figure of grain 7 in Fig. 8(7) was an exception), there are obvious variations of grain orientations from 0% to 7.5% strain due to the activations of extension twin. On the other hand, basal slipping becomes the main deformation mode for compression from 7.5% to 13.6% strain; so there are almost no variations for grain orientations. Correspondingly, the points marked with 7.5%, 11% and 13.6% overlap almost together in the {0 0 0 1} pole figures of Fig. 8.

As shown in Fig. 8, in {0 0 0 1} pole figures of every grain (the {0 0 0 1} pole figure of grain 7 in Fig. 8(7) was an exception), among points of t1–t6, it is obvious that there is one point that is nearest to the point of 7.5%, which is the point representing the extension twin variant that really activates during compression from 0% to 7.5%. In this way, the activated twin variants of every grain were determined. The results obtained from Fig. 8 agree well with that in Table 1. Shown as Fig. 8(3), for grain 3, the points of t3 and t4 are almost identically near to point of 7.5%, thus it is not convenient to determine the extension twin variant that really activate during deformation from this {0 0 0 1} pole figure, and the same inconveniency also exists in {0 0 0 1} pole figure of grain

Table 2
Extension twin variants and their orientations.

Twin variant	TT1	TT2	TT3	TT4	TT5	TT6
Orientation	$(1\,0\,\bar{1}\,2)[\bar{1}\,0\,1\,1]$	$(1\,\bar{1}\,0\,2)[\bar{1}\,1\,0\,1]$	$(0\,1\,\bar{1}\,2)[0\,\bar{1}\,1\,1]$	$(0\,\bar{1}\,1\,2)[0\,1\,\bar{1}\,1]$	$(\bar{1}\,0\,1\,2)[1\,0\,\bar{1}\,1]$	$(\bar{1}\,1\,0\,2)[1\,\bar{1}\,0\,1]$

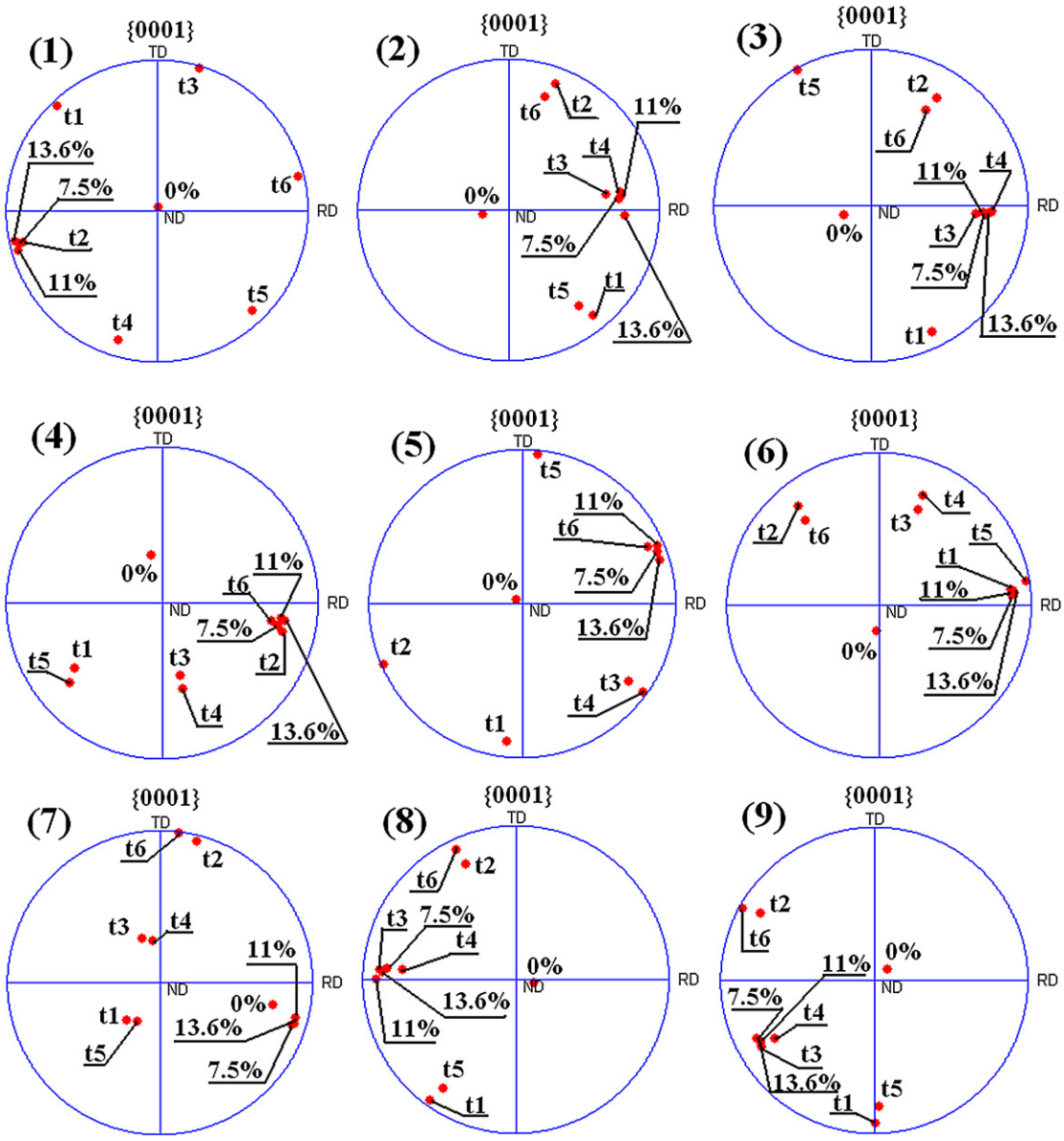

Fig. 8. The {0 0 0 1} pole figures of grains 1–9 at different strains during compression at 100 °C.

4 shown as Fig. 8(4). In Fig. 8(7), for grain 7, there is no one of points of t1–t6 that is near to point of 7.5%, thus there will not be any twin variants activated during compression from 0% to 7.5% strain, which agrees well with the corresponding result listed in Table 1.

For the specimen compressed at 170 °C, twin variants of the grains indexed by numbers from 1 to 9 in Fig. 4 were analyzed based on grain orientations corresponding to 0% and 11% strains, respectively. The results were listed in Table 3. In grains 3 and 4, similarly to grain 7 in Table 1, no twins activated from 0% to 11% strain.

Fig. 9(1)–(9) was correspondingly {0 0 0 1} pole figures of grain 1–9 in Fig. 4. Fig. 9 presents the {0 0 0 1} pole figures of the 9 grains compressed from 0% to 24.5% at 170 °C and their twin variants based on the relationship of 86.3°/⟨1 1 $\bar{2}$ 0⟩. In Fig. 9(3) and (4), the points of 0%, 11%, 16.4% and 24.5% almost overlap together which means no variations of grain orientations during compression from 0% to 24.5%, and no occurrence of twining. On the other hand, for other 7 grains, as shown in Fig. 9, there are clear variations of grain orientations from 0% to 11% strain, which means there are twins activated during this deformation process, among the points of t1–t6 that represent six extension twin variants, the twin variants can be determined according to which one is nearest to point 11%. Similarly, for the 7 grains twin variants that really activates during compression can be determined based on the twin variant that is nearest to 11% position. The results agree well with that listed in Table 2.

Table 3
Extension twin variants of grains 1–9 at 170 °C.

Grain No.	1	2	3	4	5	6	7	8	9
Twin variant	TT4	TT2	Null	Null	TT6	TT2	TT5	TT5	TT2

The above procedures about the analysis of test results were followed on for the specimen compressed at 230 °C. Twin variants of the first 9 grains (indexed by number from 1 to 9 among the 20 grains in Fig. 6) were analyzed based on grains orientation corresponding to 0% and 11.3% strains, respectively. The results show that there are not twins activated from 0% to 11.3% strain for all of the nine grains.

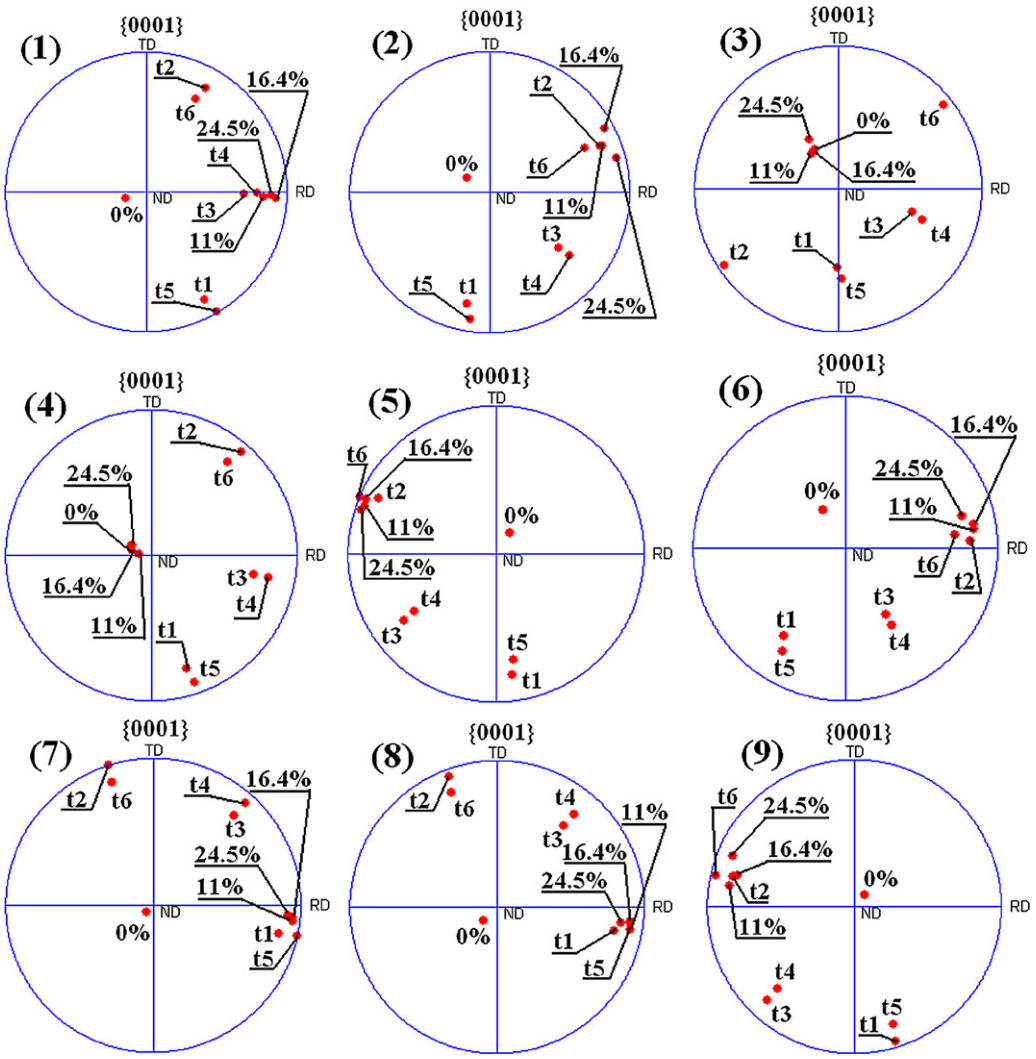

Fig. 9. The {0 0 0 1} pole figures of grains 1–9 at different strains during compression at 170 °C.

The {0 0 0 1} pole figures for the first three of the nine grains were chosen to analyze activations of twin variants in Fig. 10, Fig. 10(1)–(3) was correspondingly {0 0 0 1} pole figures of grains 1–3 in Fig. 6.

As shown in the figure, there are no obvious changes for the positions of the points corresponding to every strain, and any single point of t1–t6 points is not near to any individual points corresponding to a strain. Based on the characteristic above, it can be concluded that there are no twins activated for the three grains, which agrees well with the corresponding results described above.

For the specimen compressed at 100 °C, schmid factors of the 6 extension twin variants for grains 1–9 (the same grains are listed in Table 1) are presented in Table 4, in which the number underlined with "___" is the Schmid factor of the extension variant that really activates during deformation, and the number in '**Bold**' is the maximal Schmid factor of the 6 extension twin variants for every grain.

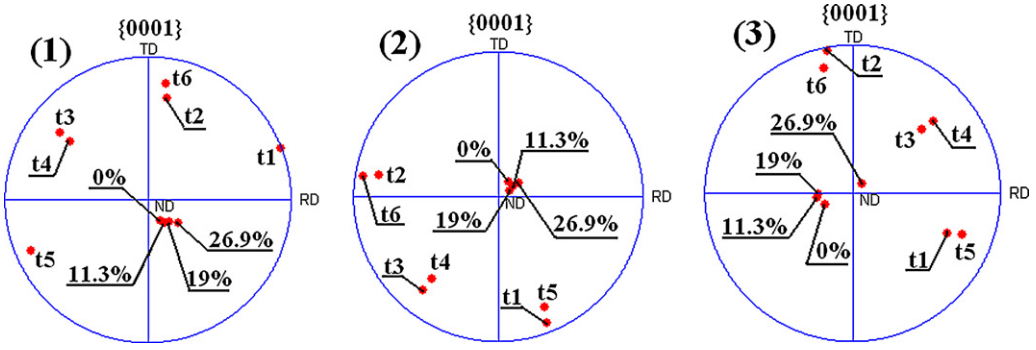

Fig. 10. The {0 0 0 1} pole figures of grains 1–3 at different strains during compression at 230 °C.

Table 4
Schmid factors of extension twin variants of grains 1–9 at 100 °C.

Grain No.	TT1	TT2	TT3	TT4	TT5	TT6
1	0.2357	0.4702	0.0402	0.0396	0.2373	**0.4724**
2	0.1128	0.0055	0.3562	0.3961	0.1386	−0.0086
3	0.0398	0.0804	0.3745	0.4140	0.0586	0.0597
4	0.2731	**0.4418**	0.0103	0.0135	0.2611	0.4265
5	0.0039	**0.4175**	0.3173	0.3245	0.0030	0.4093
6	0.4846	0.1941	0.0641	0.0655	0.4883	0.1964
7	**−0.3685**	−0.4141	−0.4249	−0.4422	−0.4089	−0.4372
8	0.1408	0.0499	0.4569	0.4282	0.1241	0.0619
9	−0.0158	0.3478	0.3447	0.3254	−0.0151	**0.3677**

Table 5
Schmid factors of extension twin variants of grains 1–9 at 170 °C.

Grain No.	TT1	TT2	TT3	TT4	TT5	TT6
1	0.0678	0.0760	0.3966	0.4325	0.0861	0.0584
2	−0.0305	0.3691	0.1982	0.2274	−0.0373	0.3331
3	−0.0581	0.2837	0.2617	**0.2979**	−0.0573	0.2483
4	0.0092	0.1826	0.3994	**0.4307**	0.0194	0.1614
5	−0.0103	0.3851	0.2856	0.2663	−0.0067	0.4079
6	0.1105	0.4456	0.0556	0.0706	0.0929	0.4130
7	0.4641	0.0417	0.2135	0.2212	0.4753	0.0452
8	0.4441	0.0428	0.1664	0.1807	0.4667	0.0511
9	0.0330	0.4491	0.2182	0.2063	0.0384	**0.4663**

As shown in Table 4, for grains 2, 3, 6, and 8, among the six twin variants of every grain, the Schmid factor of twin variant which really activates during deformation is the maximum; the twin variant with the maximal Schmid factor is not the one which really activates during deformation for grains 1, 4, 5 and 9; but the difference of Schmid factor value between them is not larger than 0.02. Taking into account the possible error of calculation on Schmid factor, it can be concluded that the activated twinning variant during deformation was the one with the maximal Schmid factor.

For the specimen compressed at 170 °C, Table 5 presents the Schmid factors of 6 extension twin variants of grains 1–9 (the same grains are listed in Table 3). For the seven grains, for which twinning was activated, the Schmid factor of twin variant which really activates during deformation is the maximal one, with the exception of grain 9. However, for this exception, the maximal Schmid factor over that of the actually activated twin variant was less than 0.025, and this verifies the relationship between the activation of twin variant and Schmid factor again. In addition, the work of Li [34] shows that, the same relationship exists between twin variant activation and Schmid factor when a rolled AZ31 sheet was compressed at room temperature.

4. Conclusions

Experimental results suggested that:

(1) Temperature plays a significant effect on texture variation during compression of AZ31 rolled sheet. For compression carried out at 100 °C, rolling texture diminished mostly at the initial phase of deformation due to large number of twins activated. When compression is carried out at 170 °C, rolling texture diminishes steadily during the whole deformation; while for compression at 230 °C, no obvious variation of rolling texture occurred due to the fact that twins are seldom activated during deformation.
(2) Tracing of the grain orientations in the scanning region during deformation with EBSD method showed that orientations had changed during the initial phase of deformation for grains with twins activated. The orientations changed little during the whole deformation for grains without twins activated.
(3) Schmid factor is the most important parameter to evaluate the twin activating. Results of tracing individual grain orientations during deformation showed that the one with the maximal Schmid factor among the six extension twin variants was typically the one that really activated.

Acknowledgement

This work has been supported by the Natural Science Foundation of China under Grant Number 50775211.

References

[1] S.H. Zhang, Z.G. Li, Y.C. Xu, L.M. Ren, Z.T. Wang, L.X. Zhou, Mater. Sci. Forum 539–543 (2007) 1753–1758.
[2] S.H. Zhang, L.M. Ren, L.X. Zhou, Mater. Sci. Forum 546–549 (2007) 333–336.
[3] E. Doege, K. Dröder, J. Mater. Process. Technol. 115 (2001) 37–47.
[4] N. Ogawa, M. Shiomi, K. Osakada, Int. J. Mach. Tool Manu. 42 (2002) 607–614.
[5] L.M. Ren, S.H. Zhang, G. Palumbo, et al., Mater. Sci. Eng. A 499 (2009) 40–44.
[6] S.H. Zhang, K. Zhang, Y.C. Xu, Z.T. Wang, Y. Xu, Z.G. Wang, J. Mater. Process. Technol. 185 (2007) 147–151.
[7] P. Yang, L. Meng, Q.-G. Xie, F.-E. Cui, Mater. Sci. Forum 546–549 (2007) 297–300.
[8] A. Jain, S.R. Agnew, Mater. Sci. Eng. A 462 (2007) 29–36.
[9] Z. Keshavarz, M.R. Barnett, Scripta Mater. 55 (2006) 915–918.
[10] O. Engler, Scripta Mater. 44 (2001) 229–236.
[11] M.R. Barnett, M.D. Nave, C.J. Bettles, Mater. Sci. Eng. A 386 (2004) 205–211.
[12] M.R. Barnett, Mater. Sci. Eng. A 464 (2007) 8–16.
[13] L. Jiang, J.J. Jonas, A.A. Luo, A.K. Sachdev, S. Godet, Scripta Mater. 54 (2006) 771–775.
[14] H.K. Lin, J.C. Huang, T.G. Langdon, Mater. Sci. Eng. A 402 (2005) 250–257.
[15] S.H. Choi, E.J. Shin, B.S. Seong, Acta Mater. 55 (2007) 4181–4192.
[16] S.H. Choi, D.H. Kim, H.W. Lee, B.S. Seong, K. Piao, R. Wagoner, Mater. Sci. Eng. A 526 (2009) 38–49.
[17] L. Jiang, J.J. Jonas, A.A. Luo, A.K. Sachdev, S. Godet, Mater. Sci. Eng. A 445 (2007) 302–309.
[18] M.D. Nave, M.R. Barnett, Scripta Mater. 51 (2004) 881–885.
[19] S.J. Liang, H. Sun, Z.Y. Liu, E.D. Wang, J. Alloys Compd. 472 (2009) 127–132.
[20] B.L. Wu, G. Wan, Y.D. Zhang, X.H. Du, F. Wagner, C. Esling, Mater. Sci. Eng. A 527 (2010) 3365–3372.
[21] H. Watanabe, M. Fukusumi, H. Somekawa, T. Mukai, Scripta Mater. 61 (2009) 883–886.
[22] L. Jiang, J.J. Jonas, R.K. Mishra, A.A. Luo, A.K. Sachdev, S. Godet, Acta Mater. 55 (2007) 3899–3910.
[23] X.S. Huang, K. Suzuki, A. Watazu, I. Shigematsu, N. Saito, J. Alloys Compd. 457 (2008) 408–412.
[24] R. Cottam, J. Robson, G. Lorimer, B. Davis, Mater. Sci. Eng. A 485 (2008) 375–382.
[25] Q.L. Jin, S.Y. Shim, S.G. Lim, Scripta Mater. 55 (2006) 843–846.
[26] J.Y. Lee, H.K. Lim, D.H. Kim, W.T. Kim, D.H. Kim, Mater. Sci. Eng. A 491 (2008) 349–355.
[27] J.A. del Valle, M.T. Pérez-Prado, O.A. Ruano, Mater. Sci. Eng. A 355 (2003) 68–78.
[28] S.B. Yi, H.G. Brokmeier, D. Letzig, J. Alloys Compd. 506 (2010) 364–371.
[29] Y.B. He, Q.L. Pan, Y.J. Qin, X.Y. Liu, W.B. Li, Y.L. Chiu, J.J. John, Chen, J. Alloys Compd. 492 (2010) 605–610.
[30] G.R. Ebrahimi, A.R. Maldar, R. Ebrahimi, A. Davoodi, J. Alloys Compd. 509 (2011) 2703–2708.
[31] S.M. Fatemi-Varzaneh, A. Zarei-Hanzaki, J.M. Cabrer, J. Alloys Compd. 509 (2011) 3806–3810.
[32] Y.N. Wang, S.B. Kang, J.Y. Cho, J. Alloys Compd. 509 (2011) 704–711.
[33] N. Tang, M.P. Wang, H.F. Lou, Y.Y. Zhao, Z. Li, Scripta Mater. 61 (2009) 223–226.
[34] Z.G. Li, The Study of Plastic Deformation Mechanism for Magnesium Alloy Sheets at Room Temperature, Ph.D. Dissertation, Institute of Metal Research, Chinese Academy Sciences, 2007.